




Observational Constraints on the Pulsar Wind Model: The Cases of Crab and Vela

Jaziel G. Coelho^{1,2} , José C. N. de Araujo², Samantha M. Ladislau², and Rafael C. Nunes²

¹Departamento de Física, Universidade Tecnológica Federal do Paraná, 85884-000 Medianeira, PR, Brazil; jazielcoelho@utfpr.edu.br

²Divisão de Astrofísica, Instituto Nacional de Pesquisas Espaciais, Avenida dos Astronautas 1758, 12227-010, São José dos Campos, SP, Brazil

Received 2021 May 28; revised 2021 August 9; accepted 2021 August 11; published 2021 October 13

Abstract

As is well known, pulsars are extremely stable rotators. However, although slowly, they spindown thanks to brake mechanisms, which are in fact still a subject of intense investigation in the literature. Since pulsars are usually modeled as highly magnetized neutron stars that emit beams of electromagnetic radiation out of their magnetic poles, it is reasonable to consider that the spindown has to do with a magnetic brake. Although an interesting and simple idea, a pure magnetic brake is not able to adequately account for the spindown rate. Thus, many alternative spindown mechanisms appear in the literature, among them the pulsar wind model, where the wind of particles coming from the pulsar itself can carry part of its rotational kinetic energy. Such a spindown mechanism depends critically on three parameters, namely, the dipole magnetic field (B), the angle between the magnetic and rotation axes (ϕ), and the density of primary particles (ζ) of the pulsar's magnetosphere. Differently from a series of articles in this subject, we consider for the first time in the literature a statistical modeling that includes a combination of a magnetic dipole and wind brakes. As a result, we are able to constrain the above referred parameters in particular for Crab and Vela pulsars.

Unified Astronomy Thesaurus concepts: [Pulsars \(1306\)](#)

1. Introduction

As is well known, pulsars, which are usually associated with rotating neutron stars (NSs), have extremely stable rotating periods. In particular the so-called rotation-powered pulsars (RPPs) emit radiation by means of their rotational kinetic energies, and as a result their periods increase, i.e., they spindown (Ostriker & Gunn 1969; Gunn & Ostriker 1969). The electromagnetic energy emitted by a pulsar, in this case, comes from its rotational kinetic energy (see, e.g., Landau & Lifshitz 1975; Padmanabhan 2001).

It is very likely that pulsars, due to their dynamic nature, should always present important temporal changes in some astrophysical quantities. In particular, increases in the rotational periods, for example, are usually quite small. The Crab pulsar (PSR B0531+21), for example, which has a period of ~ 33 ms, has a period increase rate of $\simeq 4.2 \times 10^{-13} \text{ s s}^{-1}$. While the Vela pulsar (PSR J0835-4510 or PSR B0833-45) has a spin period of ~ 89 ms and a spindown rate of $\simeq 1.25 \times 10^{-13} \text{ s s}^{-1}$.³

A long standing issue the understanding of how exactly the pulsars spindown. The magnetic dipole radiation model is a simple and interesting proposal to explain the spindown. However, such a model predicts that the brake index, a dimensionless quantity that relates the period and its first and second time derivatives, is exactly equal to three, which is not observationally corroborated. In addition to that, the estimation of the dipole magnetic field is subject to several uncertainties. For instance, several analyses suggest that the possibility of a multipolar magnetic field in highly magnetized stars should not be disregarded (see, e.g., de Lima et al. 2020). Indeed, NASA's Neutron star Interior Composition Explorer (NICER) X-ray data from PSR J0030+0451 has recently led to the first map of the hot spots on the surface of a star (see Bogdanov et al. 2019; Riley et al. 2019). The hot spots are far from antipodal,

meaning that the magnetic field structure of a pulsar is much more complex.

The fact that no pulsar has a braking index equal to three implies the need to consider more elaborate spindown models. One such a model is the so-called pulsar wind model (see Xu & Qiao 2001; Kou & Tong 2015; Tong & Kou 2017), which we consider here. We shall see later in this paper that different values of the braking index are naturally the case whenever a pulsar wind mechanism is also featured in the energy loss budget of pulsars, along with the classic magnetic dipole radiation. In addition, observations of intermittent pulsars showed explicitly the substantial role of particle wind in pulsar spindown (see Kramer et al. 2006). Magnetohydrodynamic simulations also found similar expressions to the wind braking model (see, e.g., Spitkovsky 2006). In the next section, we briefly review such a model.

It is worth mentioning that there are several scenarios that challenge the classic magnetic dipole model, like the one involving the accretion of fallback material via a circumstellar disk (Chen & Li 2016), and modified canonical models to explain the observed braking index ranges (see Allen & Horvath 1997; Magalhaes et al. 2012; Ekşi et al. 2016; de Araujo et al. 2016a, 2016b, 2016c, 2017; among others, and references therein for further models). Another interesting model for the brake is the quantum vacuum friction. We refer the reader to Coelho et al. (2016) for details. Therefore, energy loss mechanisms for pulsars are still under continuous debate.

As already mentioned we consider here the pulsar wind model, but following a different approach than that usually adopted in the literature. By means of a statistical model, we analyze in particular three relevant parameters of the wind model, namely, B , ϕ , and ζ : the dipole magnetic field, the initial angle between the rotation and magnetic axes, and the parameter related to the density of the primary particles of the magnetosphere, respectively.

This paper is organized as follows. In Section 2, we revise the pulsar wind model and in Section 3 we present the

³ For information about pulsars, we refer the reader to the Australia Telescope National Facility catalog available at: <https://www.atnf.csiro.au/research/pulsar/psrcat/>.

Table 1
Period (P), its First Derivative (\dot{P}), Surface Magnetic Field (B), Braking Index (n), and Spindown (SD) Age for the Vela and Crab Pulsars

Pulsar	P (s)	\dot{P} (10^{-13} s s $^{-1}$)	B (10^{12} G) ^a	n	Age (kyr) ^b	Ref.
PSR B0833-45 (Vela)	0.089	1.25	6.8	1.4 ± 0.2	11.3	Lyne et al. (1996); Espinoza et al. (2017)
PSR B0531+21 (Crab)	0.033	4.21	7.5	2.51 ± 0.01	0.967	Lyne et al. (1993, 2015)

Notes.

^a $B = 6.4 \times 10^{19} \sqrt{P\dot{P}}$ G for canonical parameters of M , R , and I .

^b For the Vela pulsar we use the spindown age = $P/2\dot{P}$. However, we have adopted the true age for Crab pulsar, which is known to be just 967 years because the Crab supernova was observed in 1054 CE.

statistical model to analyze the parameters B , ϕ , and ζ for the Crab and Vela pulsars. The results and discussions are presented in Section 4. The main conclusions are summarized in Section 5.

2. Pulsar Wind Model

In this section we briefly review the pulsar wind model as originally put forward by Xu & Qiao (2001) in order to elucidate the physical ideas involved.

Let us consider the pulsar as an oblique rotator that has two components of magnetic dipole: one parallel and the other perpendicular to the axis of rotation of the pulsar. The perpendicular component is responsible for the energy loss by the magnetic dipole radiation (see, e.g., Landau & Lifshitz 1975; Padmanabhan 2001), whereas the parallel component is related to the acceleration of the particles (see Li et al. 2014). Then, the phenomenon of pulsar wind is basically an energy loss mechanism due to the classic magnetic dipole radiation and particle acceleration (see Kou & Tong 2015; Tong & Kou 2017).

The energy loss due to particle wind depends on the so-called acceleration potential drop, Δv , given by (Xu & Qiao 2001)

$$\dot{E}_{\text{wind}} = 2\pi r_p^2 c \rho_e \Delta v, \quad (1)$$

where $r_p = R(R\Omega/c)^{1/2}$ is the polar gap radius, c is the speed of light, ρ_e is the primary particle density, and Δv is the corresponding acceleration potential in the acceleration gap. The density of the primary particles is related to the Goldreich-Julian charge density by $\rho_e = \zeta \rho_{\text{GJ}}$ (Goldreich & Julian 1969), where ζ is a coefficient that can be constrained by the observations. It is important to note that ζ is related to the primary particles in the acceleration gap but not to the total outflow particles.

Notice that the presence of the acceleration potential can accelerate the primary particles. Secondary particles are generated subsequently. Meanwhile, the density of the secondary particles can be much higher than the Goldreich-Julian density. In the wind braking model, all of the particles injected into the magnetosphere from the acceleration region are defined as primary particles.

If we assume that the maximum potential for a rotating dipole is given by $\Delta V = \mu\Omega^2/c^2$, it can be shown that the rotational energy loss rate reads as

$$\dot{E}_{\text{wind}} = \frac{2\mu^2\Omega^4}{3c^3} 3\zeta \frac{\Delta v}{\Delta V} \cos^2 \phi, \quad (2)$$

where $\mu = 1/2BR^3$ is the magnetic dipole moment (B is the magnetic field strength at the magnetic pole of the star and R is

the neutron star radius), Ω is the rotational frequency, and ϕ is the inclination angle between the rotational and magnetic axes.

On the other hand, as it is well known, pulsars also lose energy via classic magnetic dipole radiation (Padmanabhan 2001; Landau & Lifshitz 1975). The magnetic dipole radiation and the outflow of the particle wind may contribute independently. Then, the total rotational energy loss rate is given by Kou & Tong (2015) and Tong & Kou (2017) as

$$\dot{E} = \frac{2\mu^2\Omega^4}{3c^3} \left(\sin^2 \phi + 3\zeta \frac{\Delta v}{\Delta V} \cos^2 \phi \right) = \frac{2\mu^2\Omega^4}{3c^3} \chi. \quad (3)$$

We note that if the acceleration potential $\Delta v = 0$, then there are no particles accelerated in the gap, and the pulsar is just braking down by magnetic dipole radiation. Here χ is a dimensionless function that can be viewed as the dimensionless spindown torque. The expressions of χ for different acceleration models have been very well studied by Kou & Tong (2015; see Table 2 therein for various acceleration models). In fact, the χ parameter depends on the particle acceleration model adopted. Here, we will use the vacuum gap (VG) model with curvature radiation (CR; see Ruderman & Sutherland 1975).

We shall surmise in this work that the total energy of the star is provided by its rotational counterpart, $E_{\text{rot}} = I\Omega^2/2$, and its change is attributed to both \dot{E}_{wind} and magnetic dipole radiation. Thus, from Equation (3), the evolution of the rotational frequency of a star is given by

$$\dot{\Omega} = -\frac{B^2 R^6 \Omega^3}{6Ic^3} \chi_{\text{VG}}^{\text{CR}}, \quad (4)$$

with

$$\chi_{\text{VG}}^{\text{CR}} = \sin^2 \phi + \begin{cases} 4.96 \times 10^2 \zeta \left(1 - \frac{\Omega_{\text{death}}}{\Omega} \right) B_{12}^{-8/7} \Omega^{-15/7} & \text{if } \Omega > \Omega_{\text{death}} \\ 0 & \text{if } \Omega < \Omega_{\text{death}}, \end{cases} \quad (5)$$

where the term in parentheses accounts for the pulsar death, and B_{12} is the surface magnetic field in units of 10^{12} G. Notice that in the above equation, the term $\cos^2 \phi$, which appears in Equation (2), is now omitted. In Tong & Kou (2017), the authors argue that $\cos^2 \phi$ may not appear, in accordance with magnetospheric simulations performed by Li et al. (2012).

Consequently, the effect of pulsar death can be incorporated in the rotational energy loss rate and must be considered in modeling the long-term rotational evolution of the pulsar. Note that when a pulsar is dead ($\Omega < \Omega_{\text{death}}$), it is braked only by magnetic dipole radiation, i.e., $\chi_{\text{VG}}^{\text{CR}} = \sin^2 \phi$. Then, following the same procedure of Contopoulos & Spitkovsky (2006) and

Kou & Tong (2015), the death period ($P_{\text{death}} = 2\pi/\Omega_{\text{death}}$) is defined as

$$P_{\text{death}} = 2.8 \left(\frac{B}{10^{12} \text{G}} \right)^{1/2} \left(\frac{V_{\text{gap}}}{10^{12} \text{V}} \right)^{-1/2} s. \quad (6)$$

The inclination angle ϕ is allowed to evolve over time, and following Tong & Kou (2017), the evolution of ϕ reads as

$$\dot{\phi} = -\frac{B^2 R^6 \Omega^2}{6Ic^3} \sin \phi \cos \phi. \quad (7)$$

As already mentioned, the energy carried away by the dipole radiation and the relativistic particles originates from the rotational kinetic energy, the loss rate of which is $I\Omega\dot{\Omega}$.

Recall that the braking index is defined by

$$n = \frac{\Omega\dot{\Omega}}{\dot{\Omega}^2}. \quad (8)$$

It is interesting to note that the braking index implicitly depends on the magnetic field B , the inclination angle ϕ , and particle density ζ .

3. Statistical Models for Crab and Vela

In Kou & Tong (2015) and, in particular and mainly in Tong & Kou (2017), one sees that the key parameters to appropriately model the pulsar spindown when considering a combination of magnetic dipole and particle wind brakes are B , ϕ , and ζ .

In a modeling for the Crab pulsar, Kou & Tong (2015) assume that $B = 8.1 \times 10^{12}$ G, $\phi = 55^\circ$, and $\zeta = 10^3$. Later, Tong & Kou (2017) adopt $B \sim 10^{12}$ G, $\phi = 60^\circ$, and $\zeta = 10^2$. The authors argue that the primary particle density, ρ_e , of young pulsars is at least 80 times the ρ_{GJ} in the VG model. In fact, the particle density in the accelerating region could be $\sim 10^3$ – 10^4 times the Goldreich–Julian charge density (see also Yue et al. 2007). A much larger particle density than the Goldreich–Julian density in the pulsar magnetosphere is also found in other models and observations (Kou & Tong 2015; Tong & Kou 2017; and references therein).

Differently from these and other previous studies, we consider for the first time in the literature a statistical modeling that includes a combination of a magnetic dipole and wind brakes. We argue that a robust way to adequately obtain and constrain ϕ , ζ , and B is by means of a statistical analysis.

According to the inferred observational range of the inclination angles and the characteristic magnetic fields, we are able to constraint the ranges of the values of ϕ and ζ for a particular pulsar. As a first application of our modeling we consider the widely known Crab and Vela pulsars.

Here, we use the Markov Chain Monte Carlo (MCMC) method to analyze the parameters $\theta_i = \phi$, ζ , and B , building the posterior probability distribution function

$$p(D|\theta) \propto \exp\left(-\frac{1}{2}\chi^2\right), \quad (9)$$

where

$$\chi^2 = \left(\frac{n - n_{\text{th}}}{\sigma_n} \right)^2, \quad (10)$$

where n , n_{th} , and σ_n are the observed braking index (median value), the theoretical braking index, and the uncertainties of the observed braking index (see Table 1), respectively.

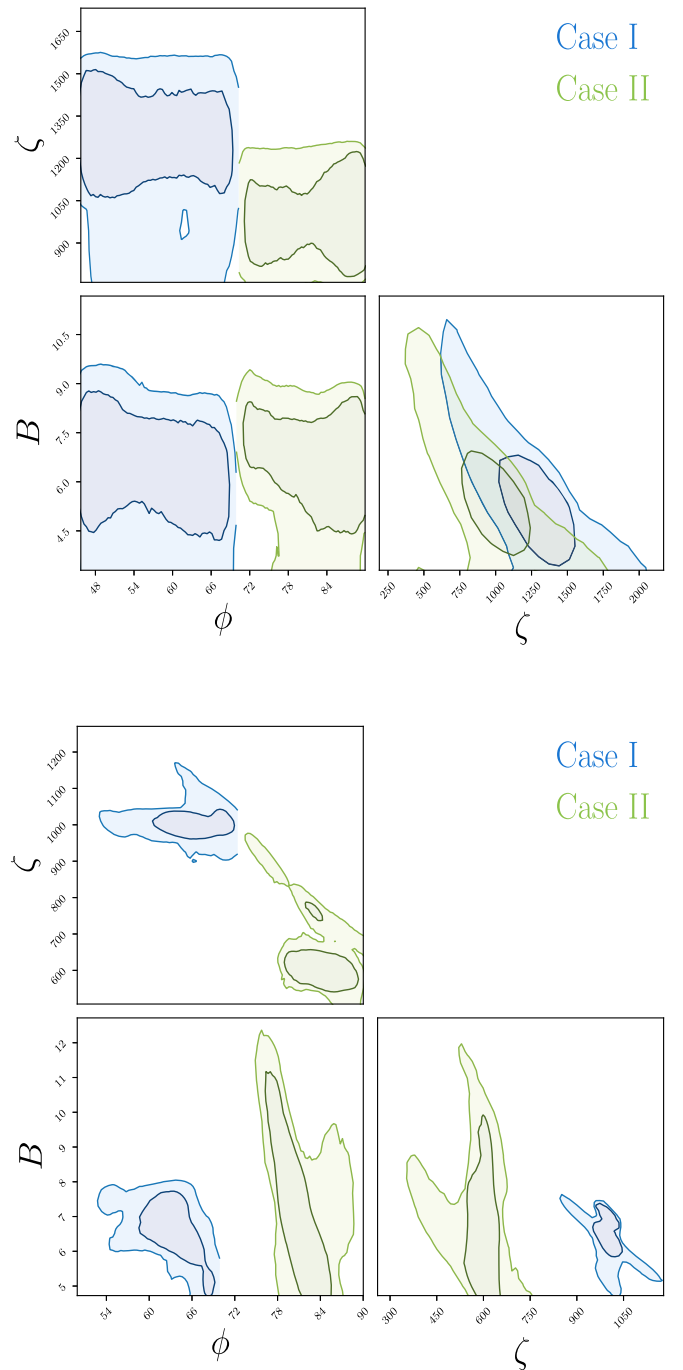


Figure 1. The parametric space at 38% CL and 68% CL, under the prior consideration $\phi \in [45^\circ, 70^\circ]$ (Case I) and $\phi \in [70^\circ, 90^\circ]$ (Case II). Upper panel: Vela pulsar. Lower panel: Crab pulsar. The parameter B is in units of 10^{12} G.

The goal of any MCMC approach is to draw M samples of θ_i from the general posterior probability density

$$p(\theta_i, \alpha|D) = \frac{1}{Z} p(\theta, \alpha) p(D|\theta, \alpha), \quad (11)$$

where $p(\theta, \alpha)$ and $p(D|\theta, \alpha)$ are the prior distribution and the likelihood function, respectively. Here, the quantities D and α are the set of observations and the possible nuisance parameters. The amount Z is a normalization term. In order to constrain the baseline θ_i , let us assume estimates of the

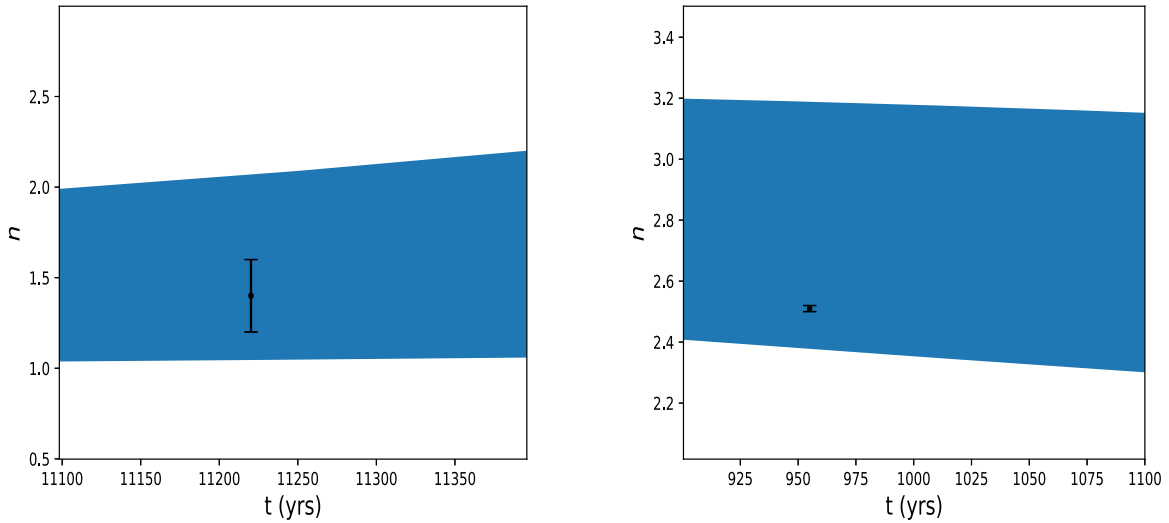


Figure 2. Statistical reconstruction at a 1σ CL of the braking index n as a function of time for Vela and Crab, on the left and right panels, respectively (Case I). The error bar in black represents the n measurements.

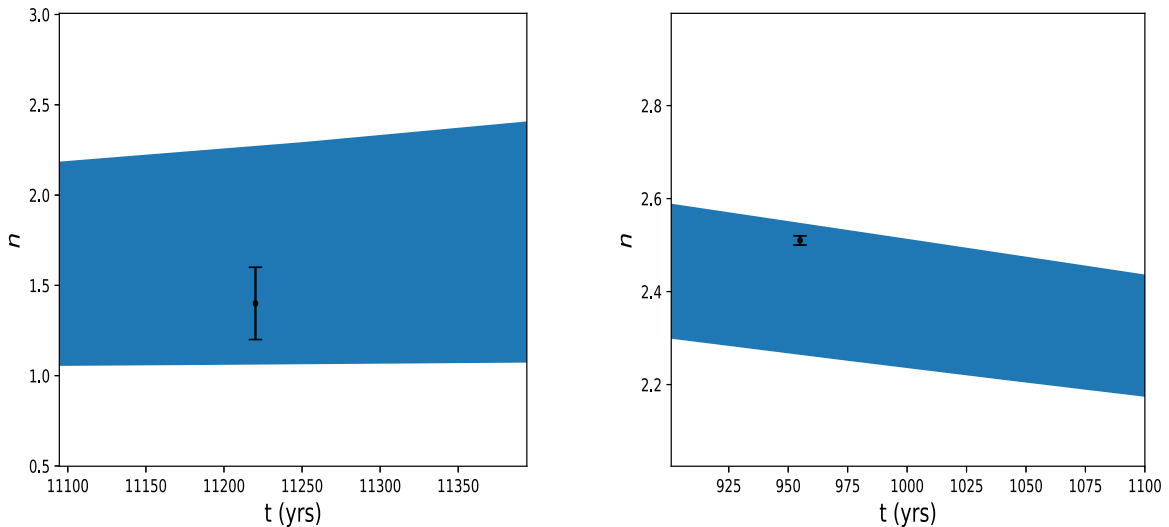


Figure 3. Statistical reconstruction at a 1σ CL of the braking index n as a function of time for Vela and Crab, on the left and right panels, respectively (Case II). The error bar in black represents the n measurements.

braking index parameters for the pulsars as follows: $n = 2.51 \pm 0.01$ for Crab and $n = 1.4 \pm 0.2$ for Vela (see Table 1).

We perform the statistical analysis based on the *emcee* algorithm (see Foreman-Mackey et al. 2013), assuming the theoretical model described in Section 2 and the following priors on the parameters baseline: first, we analyze both Vela and Crab with a uniform prior on the inclination angles of $\phi \in [45^\circ, 70^\circ]$, which are consistent with the observational constraints (Lyne et al. 2013). As a second case, we consider a uniform prior of $\phi \in [70^\circ, 90^\circ]$. In fact, the shape of the beam of the Crab pulsar has been investigated over the past few years, resulting in a range of estimates of $\phi \in [45^\circ, 70^\circ]$ (see, e.g., Dyks & Rudak 2003; Harding et al. 2008; Watters et al. 2009; Du et al. 2012). Unfortunately, at present it is impossible to accurately determine the inclination angles of the individual pulsars. Therefore, these issues are still under continuous debate (see, e.g., Lander & Jones 2018; Novoselov et al. 2020).

From the profile modeling, we can already get some information about the inclination angle. In fact, the braking index is not the only observational input, since preliminary information on ϕ is already known. Thus, we use this information as a uniform prior in our analysis. We are fitting the theoretical model under observational information quantified in terms of n , which represents in practical terms just one data point, with already known information on ϕ . Thus, we will maintain a conservative statistical limit in our results, and we will quantify all of our analyses at 38% ($\sim 0.5\sigma$) and 68% ($\sim 1\sigma$) confidence levels (CL). In what follows, let us present a summary of our main results.

4. Results and Discussions

In the following we explore the parameter space of ϕ , ζ , and B with our MCMC approach in order to constrain the probability distribution of these parameters that characterize the pulsar wind model. Then, we relax the value of B using a

uniform prior with $B \in [1, 100]$ in units of 10^{12} G. As a case study, in Figure 1 we show the parametric space on the plan ϕ - ζ at 38% and 68% CL, assuming $\phi \in [45^\circ, 70^\circ]$ (Case I) and $\phi \in [70^\circ, 90^\circ]$ (Case II).

The age of a pulsar is a useful parameter, but it is difficult to get the age from observations. Here, we have used the values showed in Table 1. For the Vela pulsar we adopted the spindown age. This age is in good agreement with independent age estimators (e.g., proper motion and supernova remnant age). It is worth mentioning that the different age estimates for both pulsars do not practically influence our statistical modeling.

For the Vela pulsar, we find $\zeta = 1280^{+350}_{-630}$ and $\zeta = 990^{+320}_{-570}$ at a 1σ CL from Cases I and II, respectively. For this inference, we find $B = 6.5^{+3.1}_{-4.4} \times 10^{12}$ G and $B = 6.8^{+2.5}_{-5.1} \times 10^{12}$ G for Cases I and II, respectively. Now, for the Crab pulsar, we find $\zeta = 1002^{+83}_{-76}$ and $\zeta = 600^{+160}_{-100}$ at a 1σ CL from Cases I and II, respectively, with $B = 6.6^{+1.2}_{-1.7} \times 10^{12}$ G and $B = 7.3^{+2.1}_{-4.3} \times 10^{12}$ G from Cases I and II, respectively. Note that the mean value of the B parameter can present statistical fluctuations along the MCMC analysis. But, as expected, these fluctuations are completely compatible with the input value. As previously mentioned, the characteristic (inferred) magnetic field from the classical magnetic dipole radiation is subject to some uncertainties. To take into account the magnetic field effects in our results, we have relaxed B using a uniform prior with $B \in [1, 100]$ in units of 10^{12} G. Nevertheless, it is worth mentioning that up to now, attempts to estimate the magnetic field strength in isolated pulsars through the measurement of cyclotron resonance features, as successfully done for accreting pulsars, have been inconclusive.

Figure 2 shows the reconstruction at a 1σ CL of the braking index n as a function of time for Vela and Crab, on the left and right panels, respectively. The reconstruction is done applying the standard propagation of error in Equation (8) from the best-fit values obtained in our analysis within the case $\phi \in [45^\circ, 70^\circ]$. Figure 3 shows the reconstruction for the second case, $\phi \in [70^\circ, 90^\circ]$. In all of our analyses, we discard the first 10% of steps of the chain as burn-in. We follow the Gelman-Rubin convergence criterion (Gelman & Rubin 1992), checking that all parameters in our chains had good convergence.

5. Final Remarks

In the literature there are several alternatives to the magnetic dipolar brake to explain the pulsar spindown, among them the pulsar wind model, where the wind of particles coming from the pulsar itself can carry part of its rotational kinetic energy. We have seen that such a spindown mechanism depends critically on three parameters, namely, the dipole magnetic field, the angle between the magnetic and rotation axes, and the density of the primary particles of the pulsar's magnetosphere.

Differently from a series of previous articles in this subject, we consider for the first time in the literature a statistical modeling that includes a combination of a magnetic dipole and particle wind brakes. Although in general there is a dependence on all of the parameters on the pulsars, we used here, without loss of generality and for the sake of exemplification, only the VG model for the particle acceleration. We emphasize that this same approach can be applied regardless of the choice of the acceleration model. As a result, we are able to constrain the

three relevant parameters of this model, i.e., B , ϕ , and ζ , in particular for Crab and Vela pulsars. This study ought to lay the groundwork for future research on the fundamental parameters of pulsar wind models and also particle acceleration.

The authors thank the referee for the comments which helped to improve the quality of the manuscript. J.G.C. is likewise grateful to the support of CNPq (421265/2018-3 and 305369/2018-0), FAPESP Project No. 2015/15897-1, and NAPI “Fenômenos Extremos do Universo” of Fundação de Apoio à Ciência, Tecnologia e Inovação do Paraná. J.C.N.A. thanks FAPESP (2013/26258-4) and CNPq (308367/2019-7) for partial financial support. R.C.N. would like to thank the agency FAPESP for financial support under the project No. 2018/18036-5.

ORCID iDs

Jaziel G. Coelho  <https://orcid.org/0000-0001-9386-1042>

References

- Allen, M. P., & Horvath, J. E. 1997, *ApJ*, 488, 409
 Bogdanov, S., Lamb, F. K., Mahmoodifar, S., et al. 2019, *ApJL*, 887, L26
 Chen, W.-C., & Li, X.-D. 2016, *MNRAS*, 455, L87
 Coelho, J. G., Pereira, J. P., & de Araujo, J. C. N. 2016, *ApJ*, 823, 97
 Contopoulos, I., & Spitkovsky, A. 2006, *ApJ*, 643, 1139
 de Araujo, J. C. N., Coelho, J. G., & Costa, C. A. 2016a, *JCAP*, 2016, 023
 de Araujo, J. C. N., Coelho, J. G., & Costa, C. A. 2016b, *ApJ*, 831, 35
 de Araujo, J. C. N., Coelho, J. G., & Costa, C. A. 2016c, *EPJC*, 76, 481
 de Araujo, J. C. N., Coelho, J. G., & Costa, C. A. 2017, *EPJC*, 77, 350
 de Lima, R. C. R., Coelho, J. G., Pereira, J. P., Rodrigues, C. V., & Rueda, J. A. 2020, *ApJ*, 889, 165
 Du, Y. J., Qiao, G. J., & Wang, W. 2012, *ApJ*, 748, 84
 Dyks, J., & Rudak, B. 2003, *ApJ*, 598, 1201
 Ekşi, K. Y., Andaç, I. C., Çikintoğlu, S., et al. 2016, *ApJ*, 823, 34
 Espinoza, C. M., Lyne, A. G., & Stappers, B. W. 2017, *MNRAS*, 466, 147
 Foreman-Mackey, D., Hogg, D. W., Lang, D., & Goodman, J. 2013, *PASP*, 125, 306
 Gelman, A., & Rubin, D. B. 1992, *StaSc*, 7, 457
 Goldreich, P., & Julian, W. H. 1969, *ApJ*, 157, 869
 Gunn, J. E., & Ostriker, J. P. 1969, *Natur*, 221, 454
 Harding, A. K., Stern, J. V., Dyks, J., & Frackowiak, M. 2008, *ApJ*, 680, 1378
 Kou, F. F., & Tong, H. 2015, *MNRAS*, 450, 1990
 Kramer, M., Lyne, A. G., O'Brien, J. T., Jordan, C. A., & Lorimer, D. R. 2006, *Sci*, 312, 549
 Landau, L. D., & Lifshitz, E. M. 1975, *The Classical Theory of Fields* (4th ed.; Oxford: Pergamon)
 Lander, S. K., & Jones, D. I. 2018, *MNRAS*, 481, 4169
 Li, J., Spitkovsky, A., & Tchekhovskoy, A. 2012, *ApJ*, 746, 60
 Li, L., Tong, H., Yan, W. M., et al. 2014, *ApJ*, 788, 16
 Lyne, A., Graham-Smith, F., Weltevrede, P., et al. 2013, *Sci*, 342, 598
 Lyne, A. G., Jordan, C. A., Graham-Smith, F., et al. 2015, *MNRAS*, 446, 857
 Lyne, A. G., Pritchard, R. S., & Graham-Smith, F. 1993, *MNRAS*, 265, 1003
 Lyne, A. G., Pritchard, R. S., Graham-Smith, F., & Camilo, F. 1996, *Natur*, 381, 497
 Magalhaes, N. S., Miranda, T. A., & Frajuca, C. 2012, *ApJ*, 755, 54
 Novoselov, E. M., Beskin, V. S., Galishnikova, A. K., Rashkovetskiy, M. M., & Biryukov, A. V. 2020, *MNRAS*, 494, 3899
 Ostriker, J. P., & Gunn, J. E. 1969, *Natur*, 223, 813
 Padmanabhan, T. 2001, *Theoretical Astrophysics—Vol. 2, Stars and Stellar Systems* (Cambridge: Cambridge Univ. Press)
 Riley, T. E., Watts, A. L., Bogdanov, S., et al. 2019, *ApJL*, 887, L21
 Ruderman, M. A., & Sutherland, P. G. 1975, *ApJ*, 196, 51
 Spitkovsky, A. 2006, *ApJL*, 648, L51
 Tong, H., & Kou, F. F. 2017, *ApJ*, 837, 117
 Watters, K. P., Romani, R. W., Weltevrede, P., & Johnston, S. 2009, *ApJ*, 695, 1289
 Xu, R. X., & Qiao, G. J. 2001, *ApJL*, 561, L85
 Yue, Y. L., Xu, R. X., & Zhu, W. W. 2007, *AdSpR*, 40, 1491